Annals of Nuclear Energy 213 (2025) 111158

Contents lists available at ScienceDirect

Annals of Nuclear Energy

journal homepage: www.elsevier.com/locate/anucene

Problem analysis and new scheme design for AB-BNCT solid Li targets

Kaiwen Qin [a,b], Nailiang Zhuang [a,b,*], Xijun Zhao [a,b], Yanting Zhang [a,b], Hangbin Zhao [b,c], Xiaobin Tang [a,b,*]

[a] Department of Nuclear Science and Technology, Nanjing University of Aeronautics and Astronautics, Nanjing 211106, China
[b] Key Laboratory of Nuclear Technology Application and Radiation Protection in Aerospace, Ministry of Industry and Information Technology, Nanjing 211106, China
[c] College of Astronautics, Nanjing University of Aeronautics and Astronautics, Nanjing 211106, China

ARTICLE INFO

Keywords:
BNCT neutron target station
Li–TiT_2 composite target
TPMS structure
Neutron yield
Heat removal capability

ABSTRACT

Neutron target stations, which are critical devices for boron neutron capture therapy (BNCT) technology, face severe problems, such as low neutron yield, poor heat removal capability, and short service life. In this study, the problems of the traditional Li target were analyzed and calculated, and a Li–TiT_2 composite target with a triply periodic minimal surface (TPMS) structured substrate was proposed to address the above issues. Simulation research on neutron distribution characteristics was conducted by using the Monte Carlo method. The heat removal capability of three TPMS (Gyroid, Diamond, and Primitive) structures and a fin structured substrate was evaluated. Results indicate that under a proton beam with an energy of 2.8 MeV and a current of 10 mA, compared with traditional Li targets, the Li–TiT_2 composite target has a neutron yield that has increased by 17.97 %, and an average neutron energy that has reduced by 2.75 %. The neutron angular distribution and neutron energy spectrum of the Li-TiT_2 composite target retain the distribution characteristics of the Li target. All three TPMS structure substrates have higher heat removal capability than the traditional fin structured substrate. Comparison with the Gyroid and Primitive substrates revealed that the Diamond substrate has the lowest peak temperature at the same proton beam intensity. The Li–TiT_2 composite target with the Diamond structure has the highest neutron yield of 2.18×10^{13} neutrons/s, which is 81.87 % higher than the maximum neutron yield of the traditional Li target with the finned structure. This research provides theoretical support and guidance for designing and developing novel neutron target stations for subsequent BNCT applications.

1. Introduction

Boron neutron capture therapy (BNCT), a type of tumor therapy that selectively kills only cancer cells without damaging healthy tissues around tumors, has received widespread attention (Shinian et al., 2022; Dymova et al., 2021). In accelerator-driven neutron source technology, neutron target stations are crucial devices wherein a proton beam bombards a metal target to produce neutrons. Accelerator neutron sources based on the ^{7}Li(p,n)^{7}Be reaction have the advantages of low reaction threshold and average neutron energy, high neutron yield, and easy moderation. They have great potential as neutron sources in accelerator-based BNCT (AB-BNCT) (Taskaev et al., 2021; Wang and Tong, 2020). However, in the proton bombardment of the Li target, more than 99.9 % of energy is deposited in the form of heat in neutron target stations (Li et al., 2021), the melting point of the solid Li target is relatively low (only 453 K), and the heat deposited by the high-energy proton beam bombarding the Li target cannot be dissipated in time. The phenomenon may cause the melting and damage of neutron target stations, hence affecting their lifespan. In particular, the requirement for the neutron yield from Li targets has increased with the increasing clinical demands of BNCT. Developing neutron target stations with high neutron yield, robust heat removal capability, and long service life is a critical issue encountered in research on accelerator-driven neutron sources for BNCT (Shinian et al., 2022).

Approaches in current research (Sato K et al., 2018; Wang et al., 2023) have focused on increasing proton beam intensity to improve the neutron yield of the ^{7}Li(p,n)^{7}Be reaction and thereby reduce the irradiation therapy time for patients. However, increasing proton beam intensity exacerbates the problems of energy deposition (Astrelin et al., 2010). Therefore, if neutron yield is to be improve by increasing the proton beam intensity, the heat removal capacity of neutron target stations should first be enhanced.

* Corresponding authors at: Department of Nuclear Science and Technology, Nanjing University of Aeronautics and Astronautics, Nanjing 211106, China.
E-mail addresses: zhuangnailiang@nuaa.edu.cn (N. Zhuang), tangxiaobin@nuaa.edu.cn (X. Tang).

https://doi.org/10.1016/j.anucene.2024.111158
Received 5 June 2024; Received in revised form 11 December 2024; Accepted 15 December 2024
Available online 19 December 2024

Various studies on improving the heat removal capability of neutron target stations have been conducted domestically and internationally. Lin et al. (Zuokang Lin and Yang, 2020) proposed replacing Li targets with Li compounds to increase the melting point of the target material. Although Li fluoride and Li oxide targets remarkably increase the melting of Li to 1121 and 1840 K, respectively, they also substantially decrease the neutron yield of the Li target to 27.7 % and 45.1 %, respectively. Li et al. (Li et al., 2021) proposed an edge-cooled target structure with cooling water flowing at the side. This cooling approach can reduce the moderation effects of traditional backside water cooling on the neutron beam and achieves a target structure temperature of less than 413.00 K under conditions of a 250 W Gaussian-distributed proton beam with a radius of 0.75 cm. Yoshihashi et al. (Yoshihashi et al., 2021) proposed incorporating V-shaped staggered ribs into smooth channel structures to enhance the heat removal capability of neutron target stations. The National Cancer Center of the United States and CICS Company of Japan collaborated to develop a conical target design scheme (Willis et al., 2008; Kaneta and Nakamura, 2023), which aims to reduce the thermal load per unit area at neutron target stations by increasing the area of proton energy deposition. Neutron Therapeutics in the USA (Koivunoro et al., 2023) proposed a design for a rotating Li target. The high-speed rotation of a neutron target station is deposited in different regions of a target disk, thereby reducing the thermal load per unit area of the neutron target station. Current designs of accelerator-driven neutron target stations enhance heat transfer by increasing heat transfer area, adding ribs and fins in cooling channels, and other traditional methods. However, the effect of conventional enhanced heat transfer approaches is limited under high proton beam fluxes.

In this study, the problems of the traditional Li target were analyzed and calculated, and a Li–TiT_2 composite target with a triply periodic minimal surface (TPMS) structure substrate was proposed to improve the neutron yield and heat removal capability of the neutron target station. The structural design and parameters of the Li–TiT_2 composite target were introduced, and the theoretical basis of the new structural design was discussed. Subsequently, a proton beam with an energy of 2.8 MeV was used to simulate the neutron yield, angular distribution, and energy spectrum of a Li–TiT_2 composite target, and the heat removal capability of three kinds of TPMS (Gyroid, Diamond and Primitive) structures and a finned structure substrate was evaluated.

2. Problems of the traditional Li target

2.1. Low utilization rate of proton beams

Common neutron production methods for accelerator neutron sources include ^{7}Li(p,n)^{7}Be (Wang et al., 2023); ^{9}Be(p,n)^{9}B (Lee et al., 2020); ^{3}H(p,n)^{3}He (Drosg, 1997); ^{9}Be(d,n)^{10}B (Capoulat et al., 2014); ^{13}C(d,n)^{14}N (Capoulat and Kreiner, 2017); ^{2}H(d,n)^{3}He (Verbeke et al., 1998), and ^{3}H(d,n)^{4}He (Fantidis and Antoniadis, 2015). Li targets have lower average neutron energy and higher neutron yield than other target materials, making them the material of choice for AB-BNCT. In this study, a proton beam with an energy of 2.8 MeV and a current of 10 mA (Zhu et al., 2024) was used to bombard the Li target in consideration of neutron economy. The proton beam was uniformly distributed, with a circular spot with a radius of 5 cm, as illustrated in Fig. 1.

The energy threshold required by the incident particle to enable a nuclear reaction to occur is expressed as (Zhu et al., 2024)

$$K_{Min} = -Q\frac{M_T + M_i}{M_T} \tag{1}$$

The nuclear reaction energy Q is given by (Zhu et al., 2024)

$$Q = [(M_i + M_T) - (M_l + M_R)]c^2 \tag{2}$$

where M_i is the mass of the incident particle, $M_i = M_p = 1.007825$ u; M_T is the mass of the target nucleus, $M_T = M_{Li} = 7.016004$ u; M_l is the mass of the outgoing particle, $M_l = M_n = 1.008665$ u; M_R is the mass of the residual nucleus, $M_R = M_{Be} = 7.016929$ u; c is the speed of light, $c^2 = 931.494$ MeV/u.

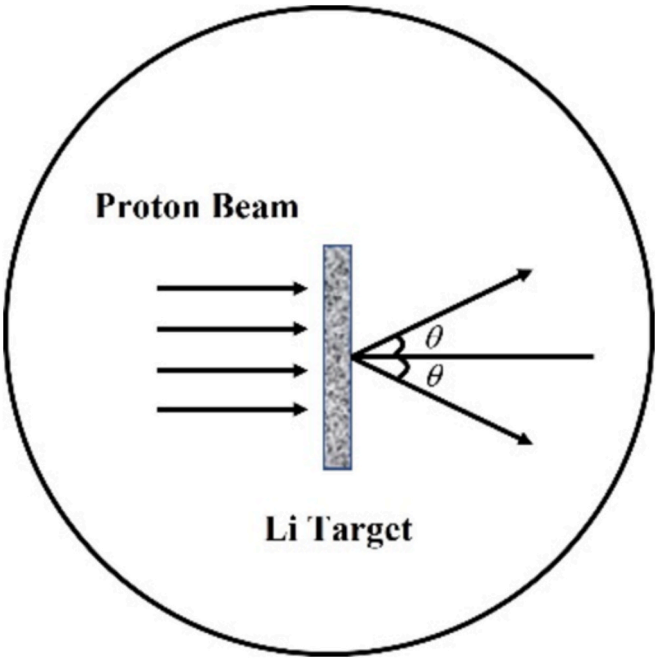

Fig. 1. Li target calculation model bombarded by a proton beam.

For the ^{7}Li(p,n)^{7}Be reaction, the nuclear reaction energy Q and energy threshold K_{Min} are − 1.64 and 1.88 MeV, respectively. This situation implies that protons with energy below this threshold cannot induce a nuclear reaction with the Li target to produce neutrons, leading to a certain degree of beam wastage.

In this study, theoretical calculations were performed on all existing nuclides to utilize protons with energies below 1.88 MeV. The nuclear reaction energy Q and energy threshold K_{Min} for the ^{3}H(p,n)^{3}He reaction is − 0.76 MeV and 1.02 MeV, respectively, with the energy threshold being lower than 1.88 MeV. The nuclear reaction cross-sections for ^{7}Li(p,n)^{7}Be and ^{3}H(p,n)^{3}He are shown in Fig. 2. The diagram indicates that in contrast to Li, protons exhibit a substantial nuclear reaction cross-section with tritium.

The concept of placing a target material containing tritium behind

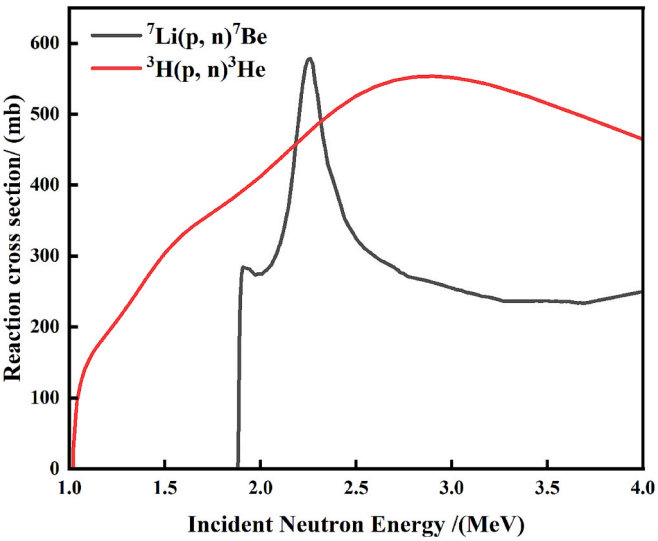

Fig. 2. Nuclear reaction cross-sections of ^{7}Li(p,n)^{7}Be and ^{3}H(p,n)^{3}He.

the traditional solid Li target was proposed in this study on the basis of the above findings. As the incident protons pass through a certain thickness of lithium layer, their energy decreases. By precisely controlling the energy of the incident proton beam and thickness of the Li layer, protons can undergo nuclear reactions with Li. The remaining energy of the proton can induce the $^{3}H(p,n)^{3}He$ reaction to produce additional neutrons. Utilizing the further $^{3}H(p,n)^{3}He$ reaction to produce neutrons on the basis of the $^{7}Li(p,n)^{7}Be$ reaction is theoretically possible, thereby increasing the neutron yield of the AB-BNCT neutron source. However, given that tritium is gaseous at normal temperature and cannot provide structural support for the Li layer, it must be adsorbed onto metallic material to form a solid target. Among the candidate metals for metal tritides, titanium has the highest hydrogen absorption density discovered thus far, reaching 9.2×10^{22} atoms/cm^3 (López-Suárez, 2017). Therefore, in this work, a Li–TiT_2 composite target was proposed to improve the neutron yield of AB-BNCT neutron target stations, as shown in Fig.3. Vanadium served as a blistering-resistant material. When a proton beam irradiates a metal, the protons that have stopped inside capture free electrons in the metal to form a hydrogen gas. Eventually, blisters and/or flakes appear on the surface as the hydrogen gas pressure rises to a level sufficient to cause ruptures (Wang et al., 2023; Kurihara et al., 2015). Copper is used as the substrate material, supporting for the Li layer and heat dissipation, and water was utilized as the coolant.

2.2. Poor heat removal ability of neutron target stations

The differential neutron yield at each proton energy is expressed as (Lee and Zhou, 1999)

$$\frac{d^2Y}{d\Omega dE_n}(\theta, E_n) = N\frac{(d\sigma_{pn}/d\Omega')(d\Omega'/d\Omega)(dE_p/dE_n)}{(-dE_p/dx)} \tag{3}$$

where $\frac{d^2Y}{d\Omega dE_n}$ is the differential neutron yield in units of neutrons per keV per solid angle per millicoulomb; N is the target atomic density; $d\sigma_{pn}/d\Omega'$ is the center-of-mass coordinate system differential (p,n) cross-section; $d\Omega$ and $d\Omega'$ are differential solid angles in the laboratory and center-of-mass coordinate systems, respectively; and $-dE_p/dx$ is the proton stopping power in the target.

Integrating Eq. (3) over energy and solid angle enables the straightforward calculation of thick target neutron energy spectra and angular distributions (Lee and Zhou, 1999):

$$\frac{dY}{dE_n}(E_n) = 2\pi\int_0^{\theta_{max}}\frac{d^2Y}{d\Omega dE_n}(\theta, E_n)\sin\theta d\theta \tag{4}$$

$$\frac{dY}{d\Omega}(\theta) = \int_{E_{n,min}}^{E_{n,max}}\frac{d^2Y}{d\Omega dE_n}(\theta, E_n)dE_n \tag{5}$$

where dY/dE_n is the energy spectrum distribution of neutron yield, and $dY/d\Omega$ is the solid angle distribution of neutron yield.

The solid angle distribution of neutron yield is converted to a radian angle distribution of neutron yield with the conversion formula:

$$\frac{dY}{d\theta} = 2\pi\sin\theta\frac{dY}{d\Omega} \tag{6}$$

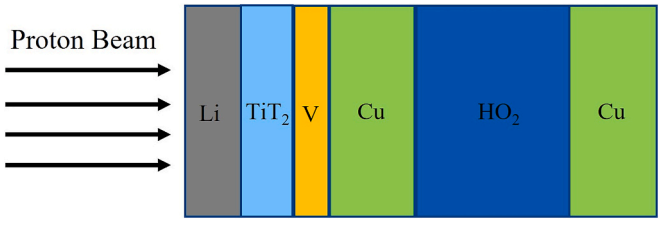

Fig. 3. Structure of the neutron target station

where $dY/d\theta$ is the radian angle distribution of neutron yield.

In this study, the neutron beam characteristics of 2.8 MeV protons bombarding the Li target were calculated on the basis of the above theory. The calculation results indicate that the neutron yield is 1.28×10^{12} neutrons/(mA·s), the maximum neutron energy is 1.10 MeV, the average neutron energy is 0.448 MeV, the neutron angle ranges from 0° to 180°, and the average neutron angle is 63.3°.

The collision between incident protons and target atoms is the main way of energy deposition method in the process of proton bombardment Li target. Proton energy is transferred either through ionization to the extranuclear electrons of the target atoms or in the form of phonons to the lattice of the target atoms. The calculation results indicate that less than 0.1 % of the incident proton energy is carried away in the form of neutrons. By contrast, more than 99.9 % of the energy is lost through the ionization effects of ions and recoil nuclei, and this energy is deposited in the form of heat in neutron target stations. However, the melting point of the solid Li target is low (only 453 K), and the heat deposited by the high-energy proton beam bombarding Li target cannot be dissipated in time. This condition may cause melting and damage of neutron target stations, thus affecting their lifespan. The peak temperature of neutron target stations must not exceed 423 K (including the safety margin) to prevent the Li target from melting (Willis et al., 2008).

The requirement for the neutron yield from Li targets has increased with the increasing clinical demands of BNCT. Developing targets with high neutron yield, robust heat removal capability, and long service life is a critical issue encountered in studies on accelerator-driven neutron sources for BNCT. Although neutron yield can be increased by increasing proton energy or beam intensity, increasing proton energy increases neutron energy, which is difficult to moderate. Therefore, approaches in current research (Sato K et al., 2018; Wang et al., 2023) have focused on increasing proton beam intensity to improve neutron yield. The neutron yield and energy deposition of a neutron target station under different proton beam intensities are shown in Fig. 4.

Fig. 4 shows that increasing proton beam intensity can increase neutron yield but also aggravates the problem of energy deposition of the neutron target station. If neutron yield is to be improve by increasing the proton beam intensity, the heat removal capacity of the neutron target station should be first be enhanced.

In recent years, TPMS structures have emerged as a hotspot in the research on enhanced heat exchange, tissue engineering, chemical engineering, and architectural structures (Feng et al., 2022; Melchels et al., 2010; Tikhonov et al., 2020; Li et al., 2019), as depicted in Fig. 5, which illustrates several typical configurations of TPMS (Dutkowski et al., 2022). Triply periodic minimal surfaces (TPMS) refers to surfaces with zero mean curvature that exhibit periodicity in three directions without

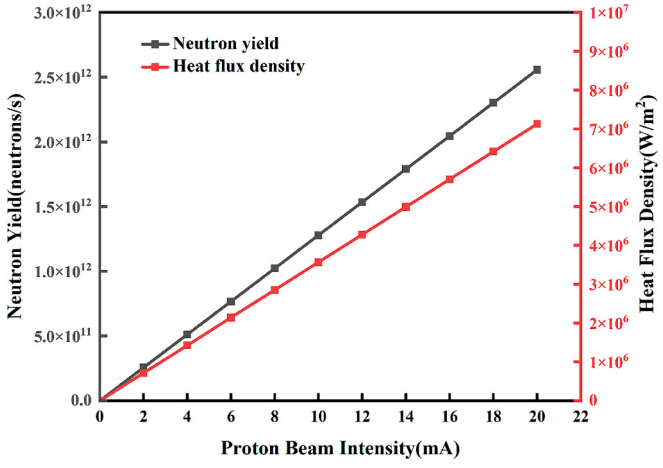

Fig. 4. Neutron yield and heat flux density of the neutron target station under different proton beam intensities.

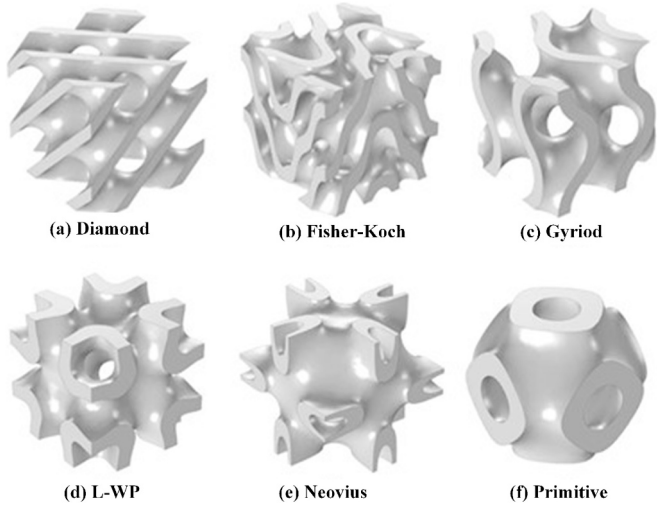

Fig. 5. TMPS structure for several functional configurations (Dutkowski et al., 2022).

self-intersection. The condition of zero mean curvature implies that the surface is smooth, whereas the periodicity and lack of self-intersections in three dimensions ensure connectivity. These unique characteristics have led to novel breakthroughs in the field of enhanced heat exchange, including thermal conduction, convection, and radiation, and also provide new ideas for the design of neutron target stations.

3. Design of the AB-BNCT Li–TiT_2 composite target

3.1. Structural design of the Li–TiT_2 composite target

In this study, the Monte Carlo program MCNP6 (Goorley, 2014) was used to establish the physical model of the Li–TiT_2 composite target to determine the thicknesses of the Li, TiT_2, and V layers that maximize the neutron yield of the AB-BNCT neutron target station. The energy loss of 2.8 MeV protons bombarding the Li–TiT_2 composite target was calculated (the nuclear reaction cross-section adopts the ENDF/-VIII.0 library and traces the transport of 10^9 particles). The calculation results are shown in Fig. 6, wherein the red curve represents the change in incident proton energy as a function of target material thickness, and the black curve represents the energy loss of protons at different thicknesses within the target material. This curve is also known as the Bragg curve.

As shown in Fig. 6(a), when the thickness of the Li layer exceeds 145 μm, the proton energy is decreases to 1.88 MeV. This reduction indicates that the neutron yield reaches its maximum value when the thickness of the Li layer exceeds 145 μm. Therefore, the thickness of the Li layer was designed to be 145 μm. A thick TiT_2 layer was added behind the 145 μm Li layer, as shown in Fig. 6(b). The proton energy at 160 μm reduced to the energy threshold of 1.02 MeV. Therefore, the thickness of the TiT_2 layer was designed to be 15 μm. Subsequently, a thick V layer was added behind the 15 μm TiT_2 layer (Fig. 6[c]). Given that the proton energy loss peaks (Bragg peak) at 168 μm, and the Bragg peak position needs to be designed in the V layer, the thickness of the V layer was designed to be 15 μm.

3.2. Characteristics of the Li–TiT_2 composite target neutron beam

The neutron yield, average neutron energy, neutron angular distribution, neutron energy spectrum and other physical quantities of Li target and Li–TiT_2 composite target were calculated by using the Monte Carlo program MCNP6 to determine whether the introduction of the TiT_2 layer affects the characteristics of the emitted neutron beam. The results show that for 2.8 MeV protons bombarding the Li and Li–TiT_2 composite target, the neutron yields and average neutron energies are 1.28×10^{12} neutrons/(mA·s) and 0.448 MeV and 1.51×10^{12} neutrons/(mA·s) and 0.436 MeV, respectively. Compared to the traditional Li target, the Li–TiT_2 composite target has increases the neutron yield by 17.97 % and reduced the average neutron energy by 2.75 %.

The neutron angular distribution and energy spectrum for 2.8 MeV protons bombarding the Li and Li–TiT_2 composite targets are shown in Fig. 7. The radian angle divides the entire counting spherical surface into 18 subintervals from the proton incidence direction, and the corresponding angle of each subinterval is 10°. The solid angle divides the entire counting spherical surface into 20 equal subintervals by area, and the neutron yield distribution of the unit solid angle can be obtained by counting the neutron yield in the subinterval.

Fig. 7 shows that the neutron angular distribution and energy spectrum of the Li–TiT_2 composite target retain the distribution characteristics of the Li target. The distribution neutron yield per radian angle is shown in Fig. 7(a). It reaches a peak in the direction of 40°, and the reduction in the direction of 90° decelerates. The neutron yield per unit solid angle distribution is shown in Fig. 7(b). The neutron yield per unit solid angle decreases gradually with the increase in angle, and the degree of decrease in the 90° direction decelerates. The neutron energy spectrum is shown in Fig. 7(c), wherein the emitted neutrons are mainly fast neutrons, and the emitted neutron energy spectrum has two peaks. Two peaks are observed because the ^{7}Li(p,n)^{7}Be reaction has two resonance peaks at 1.91 MeV and 2.26 MeV (Fig. 2).

4. Tpms-structured neutron target station

4.1. Design of the TPMS-structured substrate

Among the various TPMS structures, the Gyroid, Diamond, and Primitive structures have attracted widespread attention in previous studies due to their unique mechanical and thermophysical properties (Zhao et al., 2019; Tang et al., 2023; Laskowska et al., 2023; Kaur and Singh, 2021; Jia et al., 2020). In consideration of these characteristics, three TPMS structures with great potential in the field of convective heat transfer were selected as the research priority in this study. The mathematical control equations for three TPMS structures are provided in Eqs. (7)–(9), where L denotes the unit length of the TPMS structure, and c represents the offset of the primitive unit surface. Given that the TPMS structure varies periodically in three dimensions and its period sizes are identical, it can be formed by an array of TPMS units. The unit and array structures of the three TPMS types and their frontal views are shown in Fig. 8.

Gyroid:

$$\cos(\frac{2\pi x}{L})\cdot\sin(\frac{2\pi y}{L})+\cos(\frac{2\pi y}{L})\cdot\sin(\frac{2\pi z}{L})+\cos(\frac{2\pi z}{L})\cdot\sin(\frac{2\pi x}{L})=c \tag{7}$$

Diamond:

$$\begin{aligned}&\sin(\frac{2\pi x}{L})\sin(\frac{2\pi y}{L})\sin(\frac{2\pi z}{L})+\sin(\frac{2\pi x}{L})\cos(\frac{2\pi y}{L})\cos(\frac{2\pi z}{L})+\\&\cos(\frac{2\pi x}{L})\sin(\frac{2\pi y}{L})\cos(\frac{2\pi z}{L})+\cos(\frac{2\pi x}{L})\cos(\frac{2\pi y}{L})\sin(\frac{2\pi z}{L})=c\end{aligned} \tag{8}$$

Primitive:

$$\cos(\frac{2\pi x}{L})+\cos(\frac{2\pi y}{L})+\cos(\frac{2\pi z}{L})=c \tag{9}$$

In AB-BNCT, the thickness of the neutron target station is generally approximately 10 mm. Additive manufacturing technology recommends a wall thickness of between 0.8 and 2 mm. Therefore, the unit length L of the TPMS structure is 10 mm, and the wall thickness z is 1 mm.

The finned structure was selected for comparison with TPMS structures to evaluate the heat removal capability of TPMS structures. The design schemes of three different TPMS and finned structures within the neutron target station channel are shown in Fig. 9. The dimensions of the

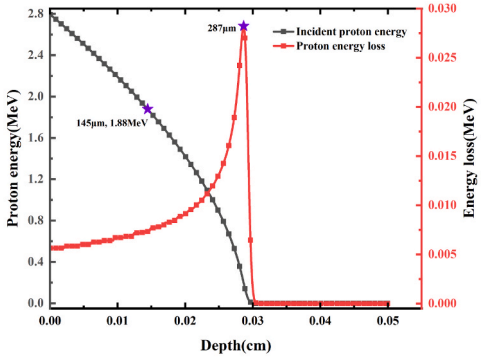

(a) 2.8 MeV proton bombardment of a thick Li layer

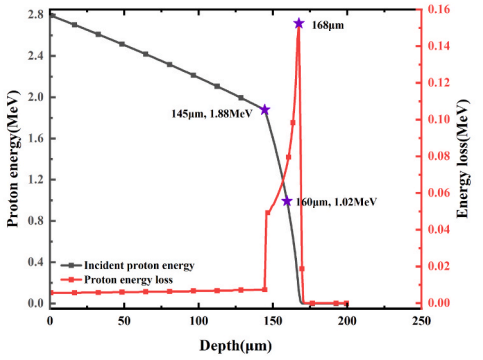

(b) 2.8 MeV proton bombardment of a composite target consisting of 145μm Li and a thick TiT_2 layer

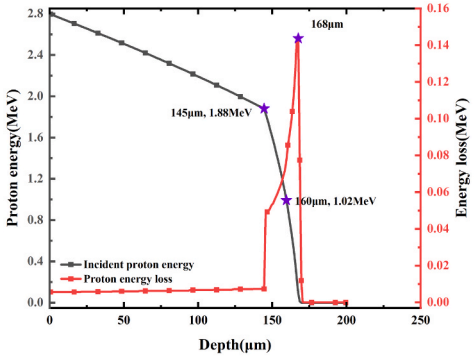

(c) 2.8 MeV proton bombardment of a composite target consisting of 145μm Li, 15μm TiT_2, and a thick V layer

Fig. 6. Energy loss curve for 2.8 MeV protons bombarding a Li–TiT_2 composite target.

neutron target station channel are 120 mm × 120 mm × 10 mm. Therefore, the three TPMS structures were designed in the form of 12 × 12 × 1 array structures. The geometric dimensions of the neutron target station with the finned structure as an example in Fig. 10.

4.2. Heat removal capacity of the TPMS structures

As described in this section, the heat removal characteristic of the neutron target station with TPMS-structured substrates was simulated and analyzed on the basis of the above designed neutron target station with the TPMS-structured substrates.

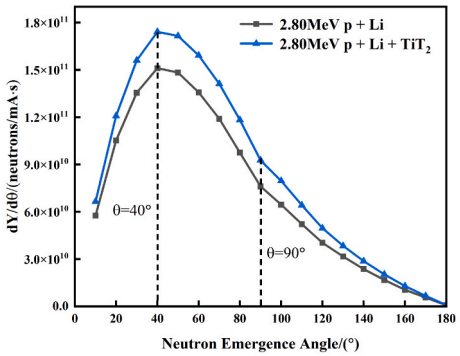

(a) Angular distribution of neutron yield normalized per unit radian angle

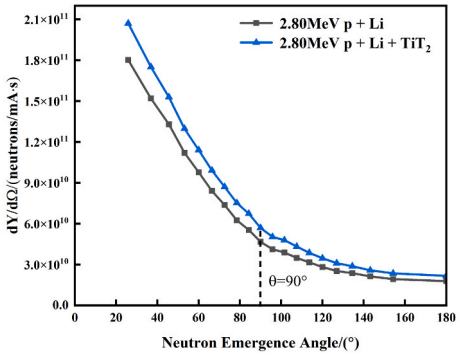

(b) Angular distribution of neutron yield normalized per unit solid angle

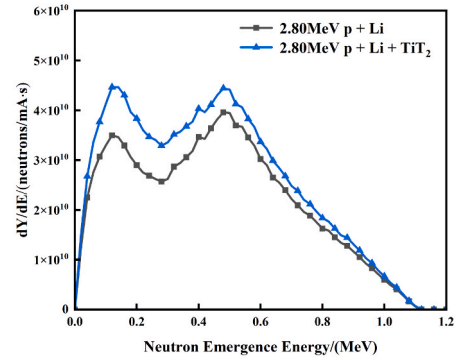

(c) Neutron energy spectrum distribution

Fig. 7. Angular distribution and energy spectrum of neutrons from Li and Li–TiT_2 composite targets.

The volume (V_s), surface area (A_s), porosity, and specific surface area of different TPMS structures are given in Table 1. Among the structures, the Diamond structure has the largest surface area, the Primitive structure exhibits the highest porosity, and the Gyroid structure has the most remarkable specific surface area.

The Reynolds number is an important parameter that describes fluid flow. According to its definition, the equation for calculating the Reynolds number is

$$\mathrm{Re} = \frac{\rho D_h v}{\mu} \tag{10}$$

where ρ represents the fluid density, D_h denotes the hydraulic diameter, v is the inlet velocity, and μ is the dynamic viscosity.

The hydraulic diameter (D_h) is calculated as (Attarzadeh et al., 2021)

$$D_h = \frac{4V_f}{A_f} \tag{11}$$

where V_f represents the volume of the liquid, and A_f denotes the wetted surface area.

The hydraulic diameters (D_h) for the Gyroid, Diamond, Primitive, and fin-shaped structures are 4.16, 3.03, 5.70 and 3.74 mm,

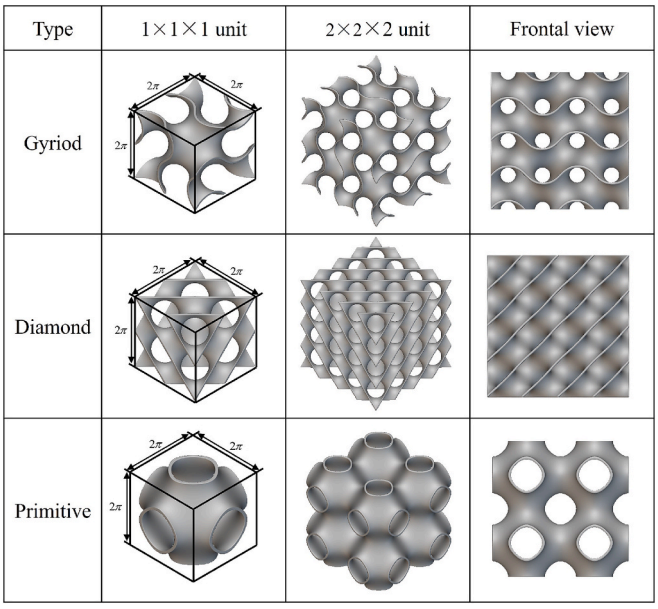

Fig. 8. Geometric models of TPMS structures.

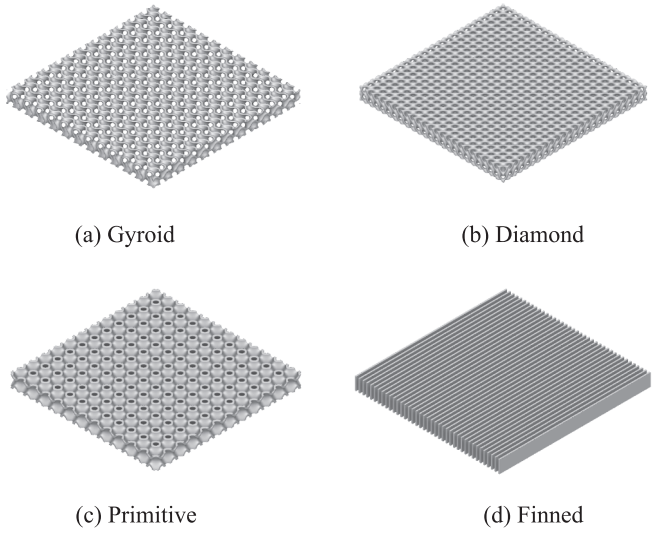

Fig. 9. Design of three TPMS and finned structures in the channel of the neutron target station.

respectively.

Under the conditions of an inlet velocity of 1 m/s and temperature range from 20–200 °C, the Reynolds numbers of Gyroid, Diamond, Primitive, and the fin-sharped structures are 4135–26 320, 3012–19 170, 5667–36 064, and 3718–23 663, respectively. These results indicate that fluid flow is turbulent under the studied conditions.

The commercial CFD software ANSYS Fluent was employed as the solver in this study (Matsson, 2023). ANSYS Fluent is widely used in engineering applications, offering various turbulence models and numerical discretization methods for effectively simulating complex fluid flow and heat transfer processes. In this simulation, the *SST k-omega* model and second-order upwind scheme of the discretization of momentum and energy equations were selected. A coupled algorithm was adopted for solution in the coupling of pressure–velocity, and the energy residual was set to 10^{-6}. The peak temperature of the Li–TiT_2 composite target with the three TPMS (Gyroid, Diamond, and Primitive) and finned structures under different proton beam intensities are shown in Fig. 11.

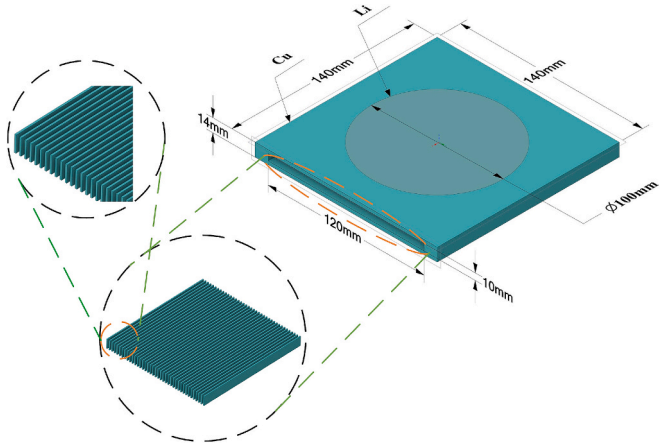

Fig. 10. Geometric dimensions of the neutron target station in AB-BNCT.

Table 1
Characteristic parameters of the TPMS structure model.

Characteristic parameter	Gyroid	Diamond	Primitive	Finned
Volume V_s (mm^3)	4.66×10^4	5.93×10^4	4.11×10^4	4.68×10^4
Surface area A_s (mm^2)	9.36×10^4	1.12×10^5	7.22×10^4	1.04×10^5
Wall thickness d (mm)	1	1	1	1
Porosity	0.676	0.588	0.715	0.675
Specific surface area (mm^{-1})	2.01	1.89	1.76	2.22

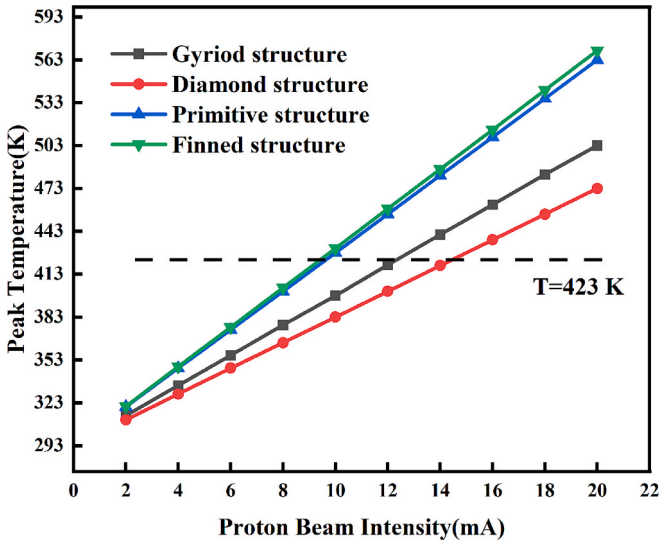

Fig. 11. Peak temperature of the Li–TiT_2 composite target with the three TPMS and finned structures under different proton beam intensities.

The results indicate that the neutron target station with the TPMS structures show a lower peak temperature than that with the finned structure at the same proton beam intensity, and the peak temperature of the Diamond structure designed for the neutron target station is lower than that of other TPMS structures.

Table 2 shows the maximum proton beam intensity and neutron yield of the Li–TiT_2 composite target with different structures can endure to ensure that the peak temperature of the neutron target station does not exceed 423 K.

The Li–TiT_2 composite target with the Diamond structure has the highest neutron yield of 2.18×10^{13} neutrons/s, which is 81.87 %

Table 2
Maximum proton beam intensity and neutron yield of the Li–TiT_2 composite target with different structures.

Characteristic parameter	Gyroid	Diamond	Primitive	Finned
Proton beam intensity(mA)	12.33	14.44	9.63	9.41
Neutron yield (neutrons/s)	1.86×10^{13}	2.18×10^{13}	1.45×10^{13}	1.42×10^{13}

higher than the maximum neutron yield (1.28×10^{12} neutrons/(mA·s) $\times$ 9.4 mA = 1.20×10^{13} neutrons/s) of the traditional Li target with the finned structure.

5. Conclusions

In this study, a Li–TiT_2 composite target with a TPMS structure substrate was proposed to improve the neutron yield and heat removal capability of the AB-BNCT neutron target stations. The evolution of the neutron field under proton beam irradiation and the enhanced heat transfer capability of the three TPMS structures and a finned structure substrate in the neutron target station were analyzed. The following main conclusions were obtained:

1) Compared with traditional Li targets, the Li–TiT_2 composite target has a neutron yield that has increased 17.97 %, and the average neutron energy that has decreased by 2.75 %. Moreover, the neutron angular distribution and energy spectrum of the Li–TiT_2 composite target retain the distribution characteristics of Li target.

2) The neutron target station with TPMS structures show a lower peak temperature than the finned structure at the same proton beam intensity, and the peak temperature of the Diamond structure designed for the neutron target station is lower than that of other TPMS structures.

3) The Li–TiT_2 composite target with the Diamond structure has the highest neutron yield of 2.18×10^{13} neutrons/s, which is 81.87 % higher than the maximum neutron yield (1.20×10^{13} neutrons/s) of the traditional Li target with the finned structure.

Declaration of competing interest

The authors declare that they have no known competing financial interests or personal relationships that could have appeared to influence the work reported in this paper.

Acknowledgments

This work was supported by the National Natural Science Foundation of China (Grant No. 12105142), the Aeronautical Science Fund (Grant No. 20240058052004), the Fundamental Research Funds for the Central University (Grant No. 56XCA2402601), the Graduate Research Innovation Program Project of Jiangsu Province (Grant No. KYCX24_0617).

Data availability

Data will be made available on request.

References

Astrelin, V.T., Burdakov, A.V., Bykov, P.V., et al., 2010. Blistering of the selected materials irradiated by intense 200 keV proton beam[J]. Journal of Nuclear Materials 396 (1), 43–48.
Attarzadeh, R., Rovira, M., Duwig, C., 2021. Design analysis of the "Schwartz D" based heat exchanger: A numerical study[J]. International Journal of Heat and Mass Transfer 177, 121415.
Capoulat, M.E., Kreiner, A.J., 2017. A 13C(d, n)-based epithermal neutron source for Boron Neutron Capture Therapy[J]. Physica Medica 33, 106–113.
Capoulat, M.E., Minsky, D.M., Kreiner, A.J., 2014. Computational assessment of deep-seated tumor treatment capability of the 9Be(d,n)10B reaction for accelerator-based Boron Neutron Capture Therapy (AB-BNCT)[J]. Physica Medica 30 (2), 133–146.
Drosg, M., 1997. Monoenergetic neutrons in the energy range from 100 eV to 200 MeV from two-body reactions with hydrogen nuclei[C]//International Conference Neutrons in Research and Industry. SPIE 2867, 490–500.
Dutkowski, K., Kruzel, M., Rokosz, K., 2022. Review of the State-of-the-Art Uses of Minimal Surfaces in Heat Transfer[J]. Energies 15 (21), 7994.
Dymova, M.A., Taskaev, S.Y., Richter, V.A., et al., 2021. Boron neutron capture therapy: current status and future perspectives[J]. Chinese Journal of Cancer 40 (1), 1–17.
Fantidis J G, Antoniadis A. Optimization study for BNCT facility based on a DT neutron generator[J]. 2015.
Feng, J., Fu, J., Yao, X., et al., 2022. Triply periodic minimal surface (TPMS) porous structures: From multi-scale design, precise additive manufacturing to multidisciplinary applications[J]. International Journal of Extreme Manufacturing 4 (2), 022001.
Goorley T. MCNP6. 1.1-beta release notes[R]. LA-UR-14-24680, 2014.
Jia, H., Lei, H., Wang, P., et al., 2020. An experimental and numerical investigation of compressive response of designed Schwarz Primitive triply periodic minimal surface with non-uniform shell thickness[J]. Extreme Mechanics Letters 37, 100671.
Kaneta, K., Nakamura, M., 2023. Proton linear accelerator and lithium target system [M]//Advances in Accelerators and Medical Physics. Academic Press 199–209.
Kaur, I., Singh, P., 2021. Flow and thermal transport characteristics of Triply-Periodic Minimal Surface (TPMS)-based gyroid and Schwarz-P cellular materials[J]. Numerical Heat Transfer, Part a: Applications 79 (8), 553–569.
Koivunoro, H., Porra, L., Joensuu, H., 2023. Description of the Accelerator-Based BNCT Project at the Helsinki University Hospital. Annex VI[M]//Advances in Boron Neutron Capture. Therapy.
Kurihara, T., Kobayashi, H., Matsumoto, H., et al., 2015. Neutron target research and development for BNCT: direct observation of proton induced blistering using light-polarization and reflectivity changes[J]. Journal of Radioanalytical and Nuclear Chemistry 305, 935–942.
Laskowska, D., Szatkiewicz, T., Bałasz, B., et al., 2023. Mechanical Properties and Energy Absorption Abilities of Diamond TPMS Cylindrical Structures Fabricated by Selective Laser Melting with 316L Stainless Steel[J]. Materials 16 (8), 3196.
Lee, S., Chang, H., Lee, J., et al., 2020. Neutron yields of Be-9 (p,xn) reactions and beam characterization for accelerator-based boron neutron capture therapy facility using MCNP6, PHITS, and GEANT4 simulation results[J]. Nuclear Instruments and Methods in Physics Research Section b: Beam Interactions with Materials and Atoms 478, 233–238.
Lee, C.L., Zhou, X.L., 1999. Thick target neutron yields for the 7Li(p, n)7Be reaction near threshold[J]. Nuclear Instruments and Methods in Physics Research Section b: Beam Interactions with Materials and Atoms 152 (1), 1–11.
Li, X., Ikeda, Y., Wang, T.K.S., et al., 2021. Study on the edge-cooling target structure for transportable accelerator-driven neutron source[J]. Nuclear Instruments and Methods in Physics Research, A 1017, 165793.
Li, L., Shi, J., Zhang, K., et al., 2019. Early osteointegration evaluation of porous Ti6Al4V scaffolds designed based on triply periodic minimal surface models[J]. Journal of Orthopaedic Translation 19, 94–105.
López-Suárez, A., 2017. Effect of absorption and desorption of hydrogen in Ti and Ti alloys[J]. New Advances in Hydrogenation Processes-Fundamentals and Applications 209–226.
Matsson, J.E., 2023. An introduction to ansys fluent 2023[M]. Sdc Publications.
Melchels, F.P.W., Barradas, A.M.C., Van Blitterswijk, C.A., et al., 2010. Effects of the architecture of tissue engineering scaffolds on cell seeding and culturing[J]. Acta Biomaterialia 6 (11), 4208–4217.
Sato K, Uritani A, Watanabe K, et al. Improved design of the exit of a beam shaping assembly for an accelerator-driven BNCT system in Nagoya University[C]// Proceedings of the international conference on neutron optics (NOP2017). 2018: 011003.
Shinian, Fu., Liang, T., Chen, H., 2022. Status and outlook: research and development on the neutron source for BNCT [J]. Chinese Science Bulletin 67 (14), 1471–1478.
Tang, W., Zhou, H., Zeng, Y., et al., 2023. Analysis on the convective heat transfer process and performance evaluation of Triply Periodic Minimal Surface (TPMS) based on Diamond, Gyroid and Iwp[J]. International Journal of Heat and Mass Transfer 201, 123642.
Taskaev, S., Berendeev, E., Bikchurina, M., et al., 2021. Neutron source based on vacuum insulated tandem accelerator and lithium target[J]. Biology 10 (5), 350.
Tikhonov, A., Evdokimov, P., Klimashina, E., et al., 2020. Stereolithographic fabrication of three-dimensional permeable scaffolds from CaP/PEGDA hydrogel biocomposites for use as bone grafts[J]. Journal of the Mechanical Behavior of Biomedical Materials 110, 103922.
Verbeke J M, Costes S V, Bleuel D, et al. Designing an epithermal neutron beam for boron neutron capture therapy for the fusion reactions 2H(d, n)3He and 3H(d, n)4He[J]. 1998.
Wang, Y.Q., Du, J.L., Lin, H., et al., 2023. An AB-BNCT epithermal neutron source using 7Li (p, n)7Be reaction[J]. Journal of Instrumentation 18 (03), P03006.
Wang, M., Tong, Y., 2020. The Progress and Prospect of Boron Neutron Capture Therapy [J]. Journal of Isotopes 33 (1), 14–26.
Willis, C., Lenz, J., Swenson, D., 2008. High-power lithium target for accelerator-based BNCT[J]. Proceedings of LINAC08 223–225.
Yoshihashi, S., Tsuneyoshi, T., Tsuchida, K., et al., 2021. High heat removal technique for a lithium neutron generation target used for an accelerator-driven BNCT system [J]. Journal of Instrumentation 16 (04), P04016.

Zhao, L., Pei, X., Jiang, L., et al., 2019. Bionic design and 3D printing of porous titanium alloy scaffolds for bone tissue repair[J]. Composites Part b: Engineering 162, 154–161.

Zhu, Y., Lin, Z., Yu, H., et al., 2024. Conceptional design of an adjustable moderator for BNCT based on a neutron source of 2.8 MeV proton bombarding with Li target[J]. Nuclear Engineering and Technology.

Zuokang Lin, Pu., Yang, Q.Z., et al., 2020. Analysis of physical design for AB-BNCT neutron target[J]. Atomic Energy Science and Technology 54 (5), 804–810.